Virtually Designed Triclosan-Based Inhibitors of Enoyl-Acyl Carrier Protein Reductase of Mycobacterium tuberculosis and of Plasmodium falciparum

6 **AUTHORS**, INCLUDING:

Fidele Ntie-Kang
Martin Luther University Halle-Wittenberg
80 PUBLICATIONS **376** CITATIONS

SEE PROFILE

Eugene Megnassan
University of Abobo-Adjamé
31 PUBLICATIONS **251** CITATIONS

SEE PROFILE

Vladimir Frecer
Slovak Academy of Sciences
62 PUBLICATIONS **696** CITATIONS

SEE PROFILE

Stanislav Miertus
International Centre For Applied Research …
182 PUBLICATIONS **8,182** CITATIONS

SEE PROFILE

Virtually Designed Triclosan-Based Inhibitors of Enoyl-Acyl Carrier Protein Reductase of *Mycobacterium tuberculosis* and of *Plasmodium falciparum*

Luc C. Owono Owono,[a, b, c] Fidele Ntie-Kang,[b, c, d] Melalie Keita,[c, e] Eugene Megnassan,*[c, e] Vladimir Frecer,[c, f, g] and Stanislav Miertus[c, g, h]

Abstract: We report here new chemical structures of predicted nanomolar triclosan-based inhibitors (TCLs) of *Mycobacterium tuberculosis* enoyl-acyl carrier protein reductase (InhA) virtually proposed by computer-assisted molecular design. 3D models of InhA-TCL complexes were prepared by in situ modifications of the reference crystal structure (PDB entry 1P45) for a training set of 15 TCLs with known InhA inhibitory activities. A QSAR model was built leading to linear correlation between the calculated free energies of complexation ($\Delta\Delta G_{com}$) and experimental values IC_{50}^{exp}: $pIC_{50} = -0.0657 \times \Delta\Delta G_{com} + 3.0502$, $R^2 = 0.96$. In addition, ligand-based quantitative pharmacophore model (PH4) was built from bound conformations of the training set compounds and confirmed the correlation between molecular models and observed activities: $pIC_{50}^{exp} = 0.8929 \times pIC_{50}^{pre} - 0.441$, $R^2 = 0.95$. Structural information from both models helped us to propose new TCL analogues. A virtual library of TCLs with known predicted activities against enoyl-acyl carrier protein reductase of *Plasmodium falciparum* (*Pf*ENR) was evaluated, revealing dual target TCLs. Moreover, analysis of binding site interactions suggested enriching substitutions, which led to more potent TCLs with predicted pIC_{50}^{pre} as low as 7 nM. The computational approach, which used both free energy estimated from molecular modeling and 3D-QSAR pharmacophore model, was helpful in virtually proposing the dual-targeted drugs and provided valuable information for the design of novel potential antituberculotic agents.

Keywords: Triclosan derivatives · InhA · QSAR model · Pharmacophore model · In silico screening · Tuberculosis · Malaria

1 Introduction

Since 1970, no new anti-TB drug has been brought into clinical practice. Despite continued research efforts and wide range of new promising molecules reported the future is expected to be bleaker than ever. According to the World Health Organization (WHO), tuberculosis (TB) has spread to every corner of the globe, reaching a level as high as 1/3 of the world population currently infected, far beyond any other infectious disease.[1] This TB burden leads to more than 5000 deaths recorded every day. The situation has been worsened by the emergence of multidrug-resistant (MDR) and extensively drug-resistant (XDR) strains of the causative agent *Mycobacterium tuberculosis* (*Mtb*)[2] in

[a] L. C. Owono Owono
University of Yaoundé I, Advanced Teacher Training College, Laboratory for Simulation and Molecular Biophysics
P.O. Box 47 Yaoundé, Cameroon

[b] L. C. Owono Owono, F. Ntie-Kang
University of Douala, Centre for Atomic Molecular Physics and Quantum Optics (CEPAMOQ)
P.O. Box 8580 Douala, Cameroon

[c] L. C. Owono Owono, F. Ntie-Kang, M. Keita, E. Megnassan, V. Frecer, S. Miertus
International Centre for Science and High Technology, UNIDO
AREA Science Park, Padriciano 99, Trieste, I-34012, Italy
phone: +22502363008

[d] F. Ntie-Kang
University of Buea, Chemical and Bioactivity Information Centre, Department of Chemistry
P.O. Box 63, Buea, Cameroon

[e] M. Keita, E. Megnassan
University of Abobo Adjamé, UFR SFA, Laboratoire de Physique Fondamentale et Appliquée
02 BP 801, Abidjan 02, Cote D'Ivoire
*e-mail: megnase@yahoo.com

[f] V. Frecer
Department of Physical Chemistry of Drugs, Faculty of Pharmacy, Comenius University
SK-83232 Bratislava, Slovakia

[g] V. Frecer, S. Miertus
International Centre for Applied Research and Sustainable Technology
SK-84104 Bratislava, Slovakia

[h] S. Miertus
Faculty of Natural Sciences, University of Ss. Cyril and Methodius
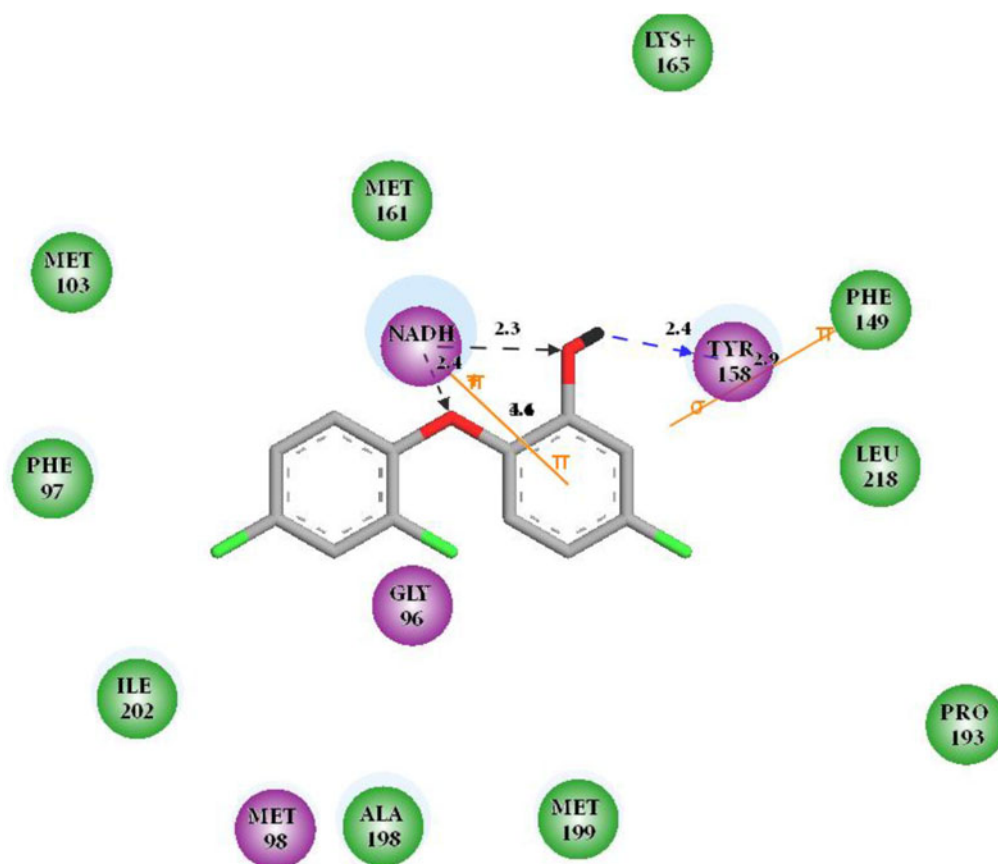SK-91701 Trnava, Slovakia

Figure 1. 2D scheme of interactions of TCL1 with residues of active site of InhA (1P45,[12]).

spite of the WHO's DOTS (directly observed treatment, short-course) Stop TB Strategy.[3] Moreover, the three key drugs, isoniazide, pyrazinamide and rifampicin, used in the DOTS regimen may lead to drug associated hepatitis.[4,5]

In response to the urgent need for new drugs against TB rational design of new molecules binding specifically to *Mtb*'s targets and exploring new scaffolds alternative to the compounds used in the clinics, has been reported.[6] Enoyl-acyl carrier protein reductase (InhA), one of the key enzymes involved in the *Mtb* mycolic fatty acid biosynthesis, has been validated as an effective target for the development of antibacterial agents.[5,7–10] Amongst monofunctional enzymes involved in the bacterial fatty acid biosynthetic pathway, the fatty acid synthase system (FAS-II), attractive drug targets for the design of new antibacterial agents can be found. These enzymes differ significantly from the type I FAS (FAS-I) present in mammals, in which all of the enzymatic activities are encoded in one or two multifunctional proteins. This distinctive difference in the FAS molecular organization between most bacteria and mammals makes the design of specific inhibitors with increased selectivity and lower toxicity possible.[11] Although genetically unrelated, both the malarial parasite *Plasmodium falciparum* (*Pf*) and *Mtb* share common enzymatic components of the FAS-II biosynthetic pathway.[12]

InhA is a well-known drug target, whose catalytic mechanism has been well studied and the catalytic role of residues Tyr158 and Lys165 has been confirmed.[13] Moreover, InhA is inhibited by adducts of the anti-TB prodrugs isoniazid (INH), ethionamide (ETA) and ethambutol (ETH). During their metabolic pathways, INH and ETA, respectively, are activated by the catalase/peroxidase enzyme KatG and the flavin monooxygenase EthA.[14–18] Since resistance to these anti-TB prodrugs is known to be linked to the requirement of prior activation, the search for InhA inhibitors that do not require activation has recently been a hot topic.[19] Triclosan (2,4,4'-trichloro-2'-hydroxydiphenyl ether, TCL), Figure 1, is known to be potent inhibitor acting against both *Pf*ENR and InhA of *Mtb* with experimental IC_{50}^{exp} of 73 and 1100 nM, respectively, binding non-covalently to both enzymes.[20] A quick comparative analysis of the crystal structures of *Pf*ENR:TCL and InhA:TCL revealed a high degree of structural conservation.[19,20] The marked difference in IC_{50}^{exp} values of TCL, and its derivatives, against these two targets could be explained by the nature of the substrate binding loop which closes upon the bound TCL within these two enzymes. While the InhA loop is occupied mostly by hydrophobic residues, that of *Pf*ENR is predominantly polar.[21,22,12] Previous works by Freundlich et al. have reported several TCL derivatives inhibiting both en-

zymes.[19,20] On the basis of these in vitro activities of TCL derivatives against *Pf*ENR, a docking-based QSAR model of TCLs binding to *Pf*ENR using a LUDI scoring function was built by our team previously to carry out in silico screening of a virtual combinatorial library of 10120 analogues.[23] This analogue-based and structure-based study resulted in a highly focused subset of 120 analogues with favorable predicted ADMET profiles with the highest predicted *Pf*ENR inhibitory potency reaching low nanomolar range (13 nM).[23] It is clearly of interest to derive another model for TCL analogues based on in vitro activities against the homologue enzyme of *Mtb* and screen this highly focused subset for probable InhA inhibitors. This was done with the goal to identify in silico hits with a potential to be developed into dual target inhibitors for both enzyme targets.
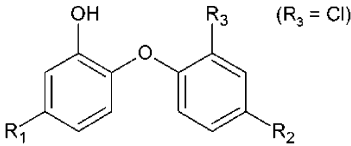
In the present work, we have built and validated a QSAR 'complexation' model based on in vitro activities (IC_{50}) of a training set (TS) of 15 selected TCLs against InhA of *Mtb*, starting from crystal structure of InhA–TCL1 complex (IC_{50} = 1100 nM, PDB entry 1P45[12]). The key ligand-receptor interactions in the active site of InhA–TCL1 complex are displayed as a 2D scheme on Figure 1. We have calculated Gibbs free energies of ligand-receptor complex formation ($\Delta\Delta G_{com}$) for the TS molecules and correlated them with the observed biological activities. The resulting quantitative structure–activity relationships model (QSAR), which employs the computed parameter $\Delta\Delta G_{com}$, was able to explain approximately 96% of the variation in the observed IC_{50}^{exp}. This QSAR model allowed structure-based design of novel TCL analogs. The identified virtual hits reached predicted inhibitory activities IC_{50}^{pre} against the InhA of *Mtb* in the low nanomolar concentration range.

In addition, training set of TCLs was used to derive a four-feature pharmacophore model (PH4) of InhA inhibitors. This pharmacophore was than matched against structural molecular data of the virtually proposed TCL analogues to confirm their compliance with the essential pharmacophoric features. The PH4 pharmacophore was also used to screen the most promising TCL analogues, inhibitors of *Pf*ENR from a previously published library,[23] for potent TCLs with a possible dual inhibitory effect against both *Pf*ENR and InhA of *Mtb*.

2 Results and Discussion

A training set of 15 TCLs and a validation set of 4 TCLs marked as VCL1-4 (Table 1) were selected from a series of compounds with experimentally determined inhibitory activities against InhA of *Mtb* originating from the same laboratory.[19] The observed activities IC_{50}^{exp} cover wide activity range from 21 to 10001 nM, which is sufficient for building a QSAR model of InhA inhibition.

Table 1. Training and validation sets of TCL inhibitors obtained from literature.

Training Set	R_1	R_2	IC_{50}^{exp} InhA[a] (nM)	IC_{50}^{exp} *Pf*ENR[b] (nM)
TCL1	—Cl	—Cl	1100	73
TCL2	—CH$_3$	—Cl	800	200
TCL3	—CH$_2$(C$_6$H$_{11}$)	—Cl	110	530
TCL4	—(CH$_2$)$_3$CH$_3$	—Cl	55	480
TCL5	—CH$_2$CH(CH$_3$)$_2$	—Cl	96	180
TCL6	—(CH$_2$)$_2$CH(CH$_3$)$_2$	—Cl	63	120
TCL7	—CH$_2$CH(CH$_3$)CH$_2$CH$_3$	—Cl	130	290
TCL8	—CH$_2$(2-Pyridyl)	—Cl	29	640
TCL9	—CH$_2$(4-Pyridyl)	—HCN	75	530
TCL10	—CH$_2$Ph	—Cl	51	71
TCL11	—(CH$_2$)$_2$Ph	—Cl	21	76
TCL12	—(CH$_2$)$_3$Ph	—Cl	50	440
TCL13	o-(CH$_3$)Ph	—Cl	1300	440
TCL14	o-(CH$_3$)Ph	—CN	10001	410
TCL15	p-F-Ph	—Cl	10001	38

Validation Set	R_1	R_2	IC_{50}^{exp} InhA[a] (nM)	IC_{50}^{exp} *Pf*ENR[b] (nM)
VCL1	—(CH$_2$)$_2$CH$_3$	—Cl	91	210
VCL2	—CH$_2$CH$_3$	—Cl	120	110
VCL3	—CH$_2$(3-Pyridyl)	—Cl	42	840
VCL4	m-(CH$_3$)Ph	—Cl	870	230

[a] Freundlich et al. [19]; [b] IC_{50}^{exp} in nM.[46–48]

2.1 QSAR Model

The relative Gibbs free energy of enzyme-inhibitor complex (*E:I*) formation from free enzyme (*E*) and free inhibitor (*I*), equation (1) in the Experimental Section, was computed for complexes prepared from the crystal structure of TCL:InhA complex[12] by in situ modification of the template inhibitor TCL in the binding site of the enzyme, as described in the Model building section. Table 2 lists the $\Delta\Delta G_{com}$ of *E:I* binding and its components, Equation 6 of Experimental Section. Since $\Delta\Delta G_{com}$ is computed in an approximate way, the relevance of the binding model was evaluated through correlation with the experimental activity data (half maximal inhibitory concentration IC_{50}^{exp}),[19] by linear regression. Plot of the linear correlation is shown on Figure 2 and statistical data of the regression are listed in Table 3. Relatively high values of the squared regression coefficient and Fischer *F*-test indicate that there is a strong correlation between the binding model (computed quantity $\Delta\Delta G_{com}$) and the observed inhibitory potencies of the TCLs. The ratio of predicted and observed inhibition constants ($pIC_{50}^{pre}/pIC_{50}^{exp}$) for the validation set of TCLs (not included into the training set) is close to one and indicates considerable predictive power of this QSAR model. Therefore, the regression equa-
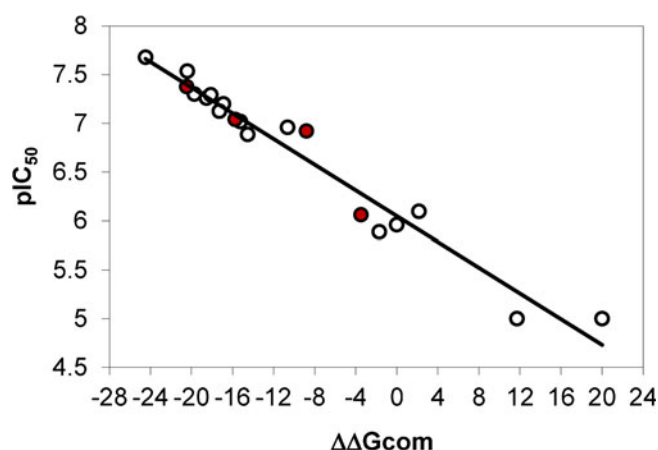
Table 2. Complexation Gibbs free energy and its components for the training set of InhA inhibitors TCL1–12.

Training Set [a]	M_w [b]	$\Delta\Delta H_{MM}$ [c]	$\Delta\Delta G_{sol}$ [d]	$-\Delta\Delta TS_{vib}$ [e]	$\Delta\Delta G_{com}$ [f]	IC_{50} exp[g]
TCL1	290	0	0	0	0	1100
TCL2	270	1.21	0.06	0.89	2.16	800
TCL3	351	−13.16	−0.19	2.72	−10.64	110
TCL4	311	−17.19	−0.27	−1.08	−18.54	55
TCL5	311	−20.76	6.39	−0.87	−15.24	96
TCL6	325	−12.84	−1.19	−2.86	−16.89	63
TCL7	325	−15.85	0.14	1.16	−14.55	130
TCL8	346	−18.14	1.56	−3.83	−20.42	29
TCL9	337	−15.95	2.49	−3.84	−17.30	75
TCL10	345	−14.58	0.09	−3.63	−18.12	51
TCL11	359	−30.16	7.11	−1.43	−24.48	21
TCL12	373	−24.04	3.71	0.61	−19.73	50
TCL13	346	−4.38	7.67	−5.01	−1.71	1300
TCL14	336	8.62	12.39	−1.01	20.01	10001
TCL15	350	6.62	5.90	−0.81	11.72	10001

Validation Set	M_w [b]	$\Delta\Delta H_{MM}$ [c]	$\Delta\Delta G_{sol}$ [d]	$-\Delta\Delta TS_{vib}$ [e]	$\Delta\Delta G_{com}$ [f]	pIC_{50} pre/ pIC_{50} exp [h]
VCL1	297	−16.80	1.08	−0.04	−15.76	1.016
VCL2	283	−21.35	12.01	0.54	−8.80	0.935
VCL3	348	−18.31	1.67	−3.85	−20.49	1.007
VCL4	346	0.64	−0.22	−3.92	−3.50	1.072

[a] for the chemical structures of the training set of inhibitors see Table 1. [b] M_w is the molecular mass of inhibitors. [c] $\Delta\Delta H_{MM}$ is the relative enthalpic contribution to the Gibbs free energy change related to $E{:}I$ complex formation derived by molecular mechanics (MM): $\Delta\Delta H_{MM}\cong[E_{MM}\{E{:}I_x\}-E_{MM}\{I_x\}]-[E_{MM}\{E{:}I_{ref}\}-E_{MM}\{I_{ref}\}]$, I_{ref} is the reference inhibitor TCL1; [d] $\Delta\Delta G_{sol}$ is the relative solvation Gibbs free energy contribution to the Gibbs free energy change related to $E{:}I$ complex formation: $\Delta\Delta G_{sol}=[G_{sol}\{E{:}I_x\}-G_{sol}\{I_x\}]-[G_{sol}\{E{:}I_{ref}\}-G_{sol}\{I_{ref}\}]$, [e] $-\Delta\Delta TS_{vib}$ is the relative entropic contribution of the inhibitor to the Gibbs free energy related to $E{:}I$ complex formation: $\Delta\Delta TS_{vib}=[\Delta\Delta TS_{vib}\{I_x\}_E-\Delta\Delta TS_{vib}\{I_x\}]-[\Delta\Delta TS_{vib}\{I_{ref}\}_E-\Delta\Delta TS_{vib}\{I_{ref}\}]$ [f] $\Delta\Delta G_{com}$ is the relative Gibbs free energy change related to $E{:}I$ complex formation: $\Delta\Delta G_{com}\cong\Delta\Delta H_{MM}+\Delta\Delta G_{sol}-\Delta\Delta TS_{vib}$. [g] IC_{50} exp is the experimental InhA half maximal inhibition concentration obtained from Reference[19] [h] ratio of predicted and experimental half maximal inhibition concentrations pIC_{50} pre/pIC_{50} exp. pIC_{50} pre was predicted from computed $\Delta\Delta G_{com}$ using the regression equation for InhA shown in Table 3.

Figure 2. Plot of the correlation equation between pIC_{50} exp and relative complexation Gibbs free energies $\Delta\Delta G_{com}$ (in kcal/mol) of the TS molecules. The data for the validation set are in red color.

logues inhibiting thymidine monophosphate kinase of *Mtb*.[28] In another example, a computational design study resulted in a mechanistic insight into selectivity of modified statine core peptidomimetic inhibitors of plasmepsin II of *P. falciparum* over human cathepsin D.[29]

2.2 Binding Mode of Inhibitors

The binding mode of TCLs derived from the the InhA:TCLₓ crystal structures[12,19] and complexation model are illustrated on Figures 3–5. The interactions of inhibitors at the active site of InhA of *Mtb* reported in the reference X-ray structure of TCL (Figure 1,[12]), namely the π–π stacking with the pyridyl ring of NADH and cation–π interaction with the pyridin nitrogen of NADH, are conserved. In addition, hydrogen bond (HB) involving the hydroxyl group of TCL and Tyr158 (Figures 2 and 3), is also preserved.

The consistency of the QSAR model of InhA inhibition by TCLs, with $E{:}I$ complexes generated by *in situ* modification of bound reference inhibitor, was validated by comparison of generated bound conformation of the most active inhibitor TCL16 with the actual relaxed crystal structure obtained from PDB (3FNH).[19] As we can see from Figure 4 the superimposition of both ligands in their bound conformations displays only a minor *RMSD* of 0.72 Å (calculated for all atoms) and exhibits a small deviations of the phenyl ring orientation with a torsion angle difference of less than 30°.

Let us recall that one of the main contributions to enzyme-inhibitor interaction of TCL analogs in *Pf*ENR involves the hydrophobic pocket formed by residues Tyr267, Val274, Tyr277, Ile323, Phe325 and Ile326.[23] In the InhA of *Mtb*, these residues are replaced by Phe149, Tyr158, Pro193, Ile194, Trp222, Leu217 and Leu218.[19] As we can see on Figure 5A for inhibitor TCL11 the hydrophobic R_1 substituent $-(CH_2)_2Ph$ reaches that hydrophobic pocket and contributes significantly to the stabilizing interaction in the active site of InhA.

tion 7 (Table 3) and the computed $\Delta\Delta G_{com}$ quantities of novel TCL analogues can be used for prediction of their InhA inhibitory concentrations (IC_{50} pre), provided that these analogues share the same binding mode with the training set compounds.

This computational approach typically shortens the route to discovery of new lead compounds and saves time compared with the traditional approach, as it was observed for design of peptidic and peptidomimetic inhibitors of HIV-1 protease.[24,25] Further examples of successful computational derivation are inhibitors of hepatitis C virus (HCV) protease,[26] combinatorial design of bicyclic thymidine analogues[27] and structure-based design of thymidine ana-

Table 3. Statistical data of correlation between computed $\triangle\triangle G_{com}$ of training set inhibitors and their experimental activities IC_{50}^{exp} against the InhA of *Mtb*.

Correlation equation: $pIC_{50} = -0.0657 \times \triangle\triangle G_{com} + 3.0502$ (7)

Statistical data of the regression:	
Number of compounds n	15
Squared correlation coefficient of regression R^2	0.96
Leave-one-out cross-validated squared correlation coefficient R^2_{XV}	0.93
Standard error of the regression σ	0.166
Statistical significance of regression, Fisher F-test	371.7
Level of statistical significance α	$>95\%$
Range of activity of IC_{50}^{exp} (nM)	21–10001

Figure 4. Superimposition of bound conformations of TCL16 prepared by in situ modification of the crystal structure of TCL:InhA (1P45)[12] with the same ligand in crystal structure of its complex with InhA of *Mtb* (3FNH).[19] Calculated RMSD is equal to 0.72 Å.

While in *Pf*ENR the R$_2$ group of TCL analogs is surrounded by active site residues Asn218, Val222, Met281 as well as the substrate binding loop residues Ala319 and Ile323. In InhA of *Mtb* this group is surrounded by Ala198, Ile202 and Phe97 side chains. The R$_3$ group of TCL analogs tested as *Pf*ENR inhibitors contains amines which interact mainly with the NAD$^+$ co-factor as well as with residues of the binding loop Ser317, Ala319, Ala320 and solvent.[23] In InhA of *Mtb* the R$_3$ group binds mainly to residues Ser20 and Gly96.

Further enrichment of considered enzyme-inhibitor interactions by new substitutions in TCL analogs with the same mode of InhA binding will lead to improved predicted potencies of the new structurally similar compounds, provided that the predictive power of the correlation eq. 7 holds also beyond the range of activities of the training set.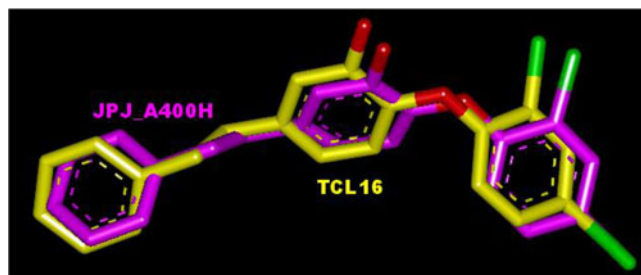 The predictive ability of our QSAR model relying on the computed $\triangle\triangle G_{com}$ was also confirmed by the PH4 pharmacophore model of the InhA inhibitory activity.

2.3 "Ligand-Based" 3D QSAR Pharmacophore Model

The 3D-QSAR PH4 pharmacophore generation process follows three main steps: (i) the constructive step, (ii) the subtractive step, and (iii) the optimization step.[41] The constructive phase of HypoGen automatically selected the most active compounds for which $IC_{50}^{exp} \leq 2 \times 21$ nM as leads. Thus, TCL8 (29 nM) and TCL11 (21 nM) were used to generate the starting PH4 features. Only those features were retained which matched both leads. In the subtractive phase, which is normally used to remove pharmacophoric features present in poorly active molecules, none of the training set compounds were found inactive ($IC_{50}^{exp} > 21 \times 10^{3.5}$ nM). During the optimization phase, the pharmacophoric hypothesis score is improved. Hypotheses are scored accord-

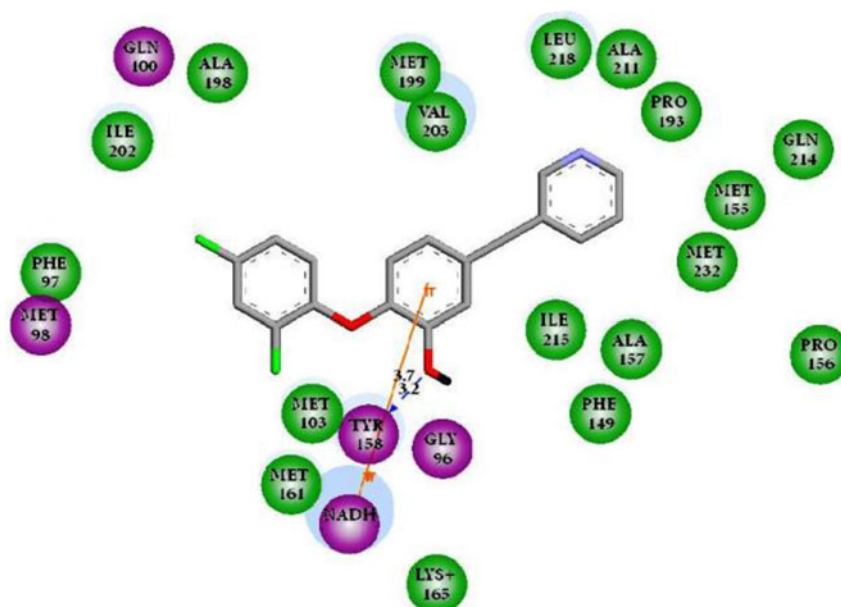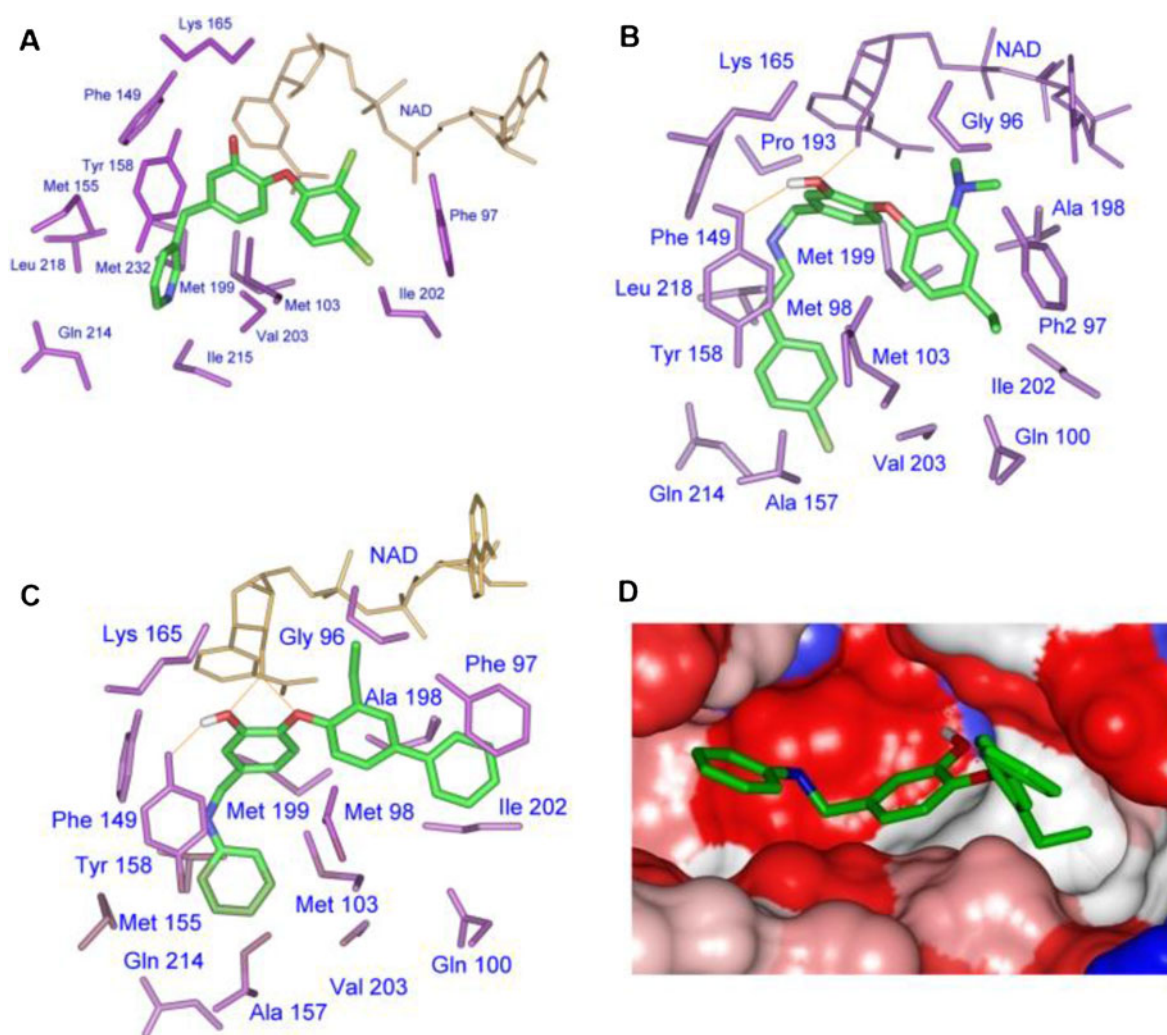**Figure 3.** 2D scheme of interactions of TCL11 with residues of active site of InhA.

Figure 5. Close-up of (A) TCL11, (B) TCL-40-9-11 and (C) TCL-36-23-9 at the active site of InhA of *Mtb*. Hydrogen bonds are shown in orange color and InhA residues are in purple color. (D) Connolly surface of the same active site with TCL-36-23-9. The binding cleft surface is colored according to residue hydrophobicity: red – hydrophobic, blue – hydrophilic and white – intermediate residues.

ing to errors in activity estimates from regression and complexity via a simulated annealing approach. At the end of the optimization the top scoring 10 unique pharmacophoric hypotheses were kept, all displaying four features.

The generated pharmacophore models were then assessed for their reliability based on the calculated cost parameters.

The overall costs ranged from 62.1 (Hypo1) to 148.0 (Hypo10). The relatively small gap between the highest and lowest cost parameter corresponds well with the homogeneity of the generated hypotheses and the consistency of the training set. For this PH4 model the fixed cost (34.2) is lower than the null cost (244.2) by a difference of $\triangle = 210$. This difference is a major quality indicator of the PH4 predictability ($\triangle > 70$ corresponds to an excellent chance or a probability higher than 90% that the model represents a true correlation[41]). To be statistically significant the hypotheses have to be as close as possible to the fixed cost and as far as possible from the null cost. For the set of 10 hypotheses $\triangle \geq 96.2$ which attests the high quality of the pharmacophore model.

The standard indicators as the root-mean-square deviations (*RMSD*) between the hypotheses ranged from 2.067 to 4.147 and the squared correlation coefficient (R^2) falls to an interval from 0.88 to 0.49. The first PH4 hypothesis with the best *RMSD* and R^2 was retained for further analysis. The statistical data for the set of hypotheses (costs, *RMSD*, R^2) are listed in Table 5. The geometry of the Hypo1 pharmacophore of InhA inhibition is displayed on Figure 6. The regression equation for pIC_{50}^{exp} vs. pIC_{50}^{pre} estimated from Hypo1: $pIC_{50}^{exp} = 0.8929 \times pIC_{50}^{pre} + 0.441$ ($n = 15$, $R^2 = 0.95$, $R_{xv}^2 = 0.92$, *F*-test = 294.2, $\sigma = 0.186$, $\alpha > 95\%$) is plotted in Figure 7. To check the consistency of the generated pharmacophore model we have computed the ratio of predicted and observed activities ($pIC_{50}^{pre}/pIC_{50}^{exp}$) for the validation set. The computed ratios are as follows: VCL1 0.84,
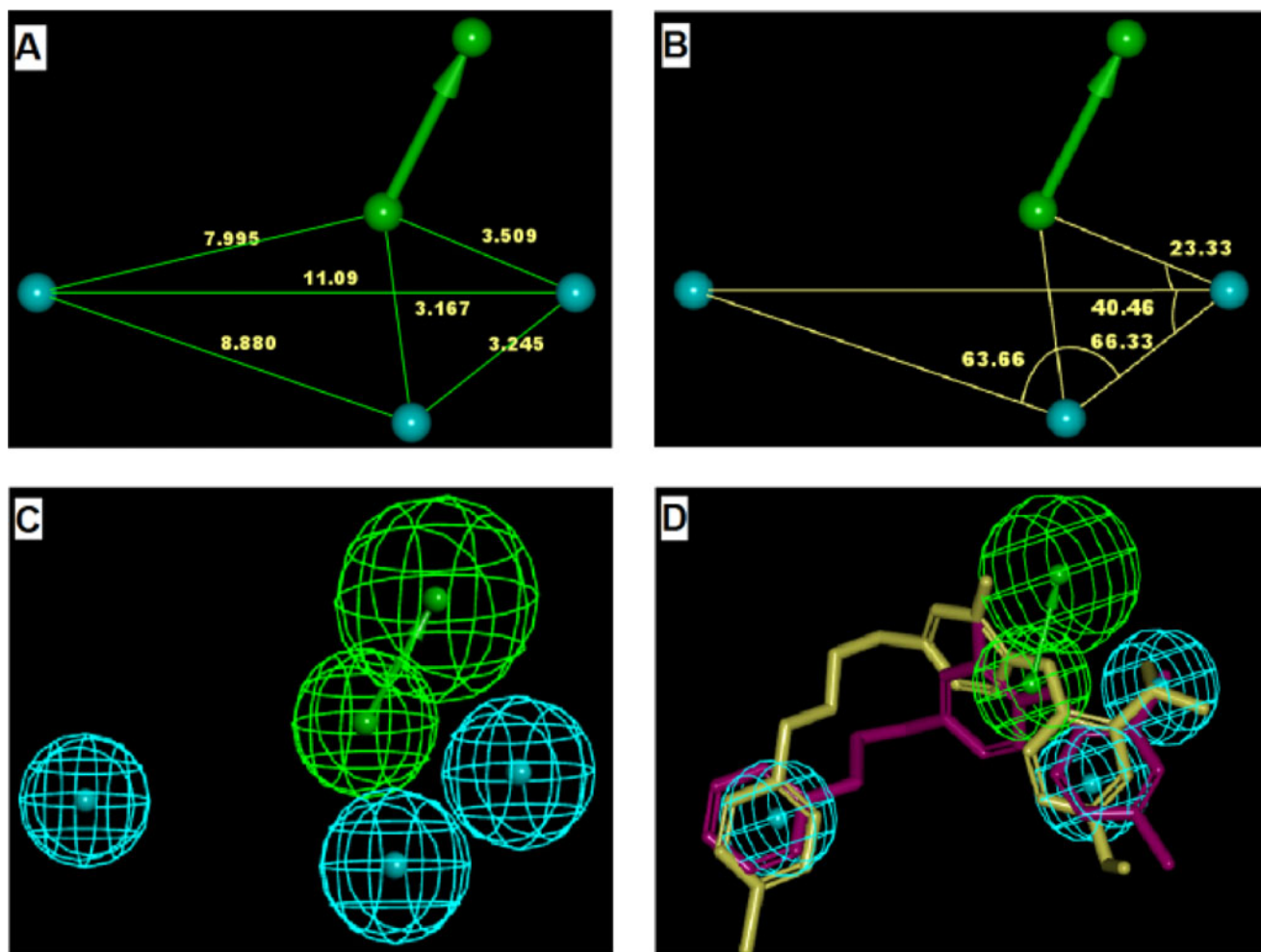
Figure 6. (A,B) Coordinates of the Hypo1 pharmacophore of InhA inhibition, (C) features of the pharmacophore of InhA inhibition, (D) pharmacophore mapping with TCL12 (purple) and TCL-40-9-11 (yellow). Color legend of features: hydrophobic (blue), acceptor (green).

VCL2 0.78, VCL3 1.03, VCL4 1.1 all of them relatively close to one, which documents substantial predictive power of the regression for the best PH4 model.

The randomization validation of the PH4 model was carried out by the CatScramble algorithm of the Catalyst for 49 random runs corresponding to a 98 % confidence level. This procedure created 10 valid hypotheses for each run. However, none of them was as predictive as Hypo10 the hypothesis with the highest cost of the ten best hypotheses generated and shown in Table 5. Thus there is a 98 % probability that the best selected hypothesis Hypo1 represents a pharmacophore model for inhibitory activity of TCLs with a similar level of predictive power as the complexation QSAR model, which relies on the 3D structures of the InhA:TCL$_x$ complexes and computed Gibbs free energies of enzyme-inhibitor binding $\Delta\Delta G_{com}$.

We have carried out computational design and selection of new TCL analogues with predicted elevated inhibition potencies against the InhA of *Mtb*, which was based mainly on the presence of the hydrophobic feature included in the best PH4 pharmacophore model at the position of R$_1$ group (Table 1). The selection was made from a virtual library of TCLs with predicted antimalarial activity listed in the Reference.[23]

2.4 In Silico Screening of Virtual library of TCLs Inhibiting *Pf*ENR

In a recent study on antimalarial effects of TCLs[23] we have proposed a highly focused virtual combinatorial subset containing 120 TCLs, which were predicted to possess inhibitory activities against *Pf*ENR in the nanomolar concentration range. In this work, we have performed in silico screening of that subset of TCL analogs by employing the QSAR model relying on computed values of $\Delta\Delta G_{com}$ with the aim to identify compounds that are active both against *Pf*ENR and the InhA of *Mtb* at the same time. The *R*-groups R$_1$, R$_2$ and R$_3$ of the virtual subset are displayed on Figure 8
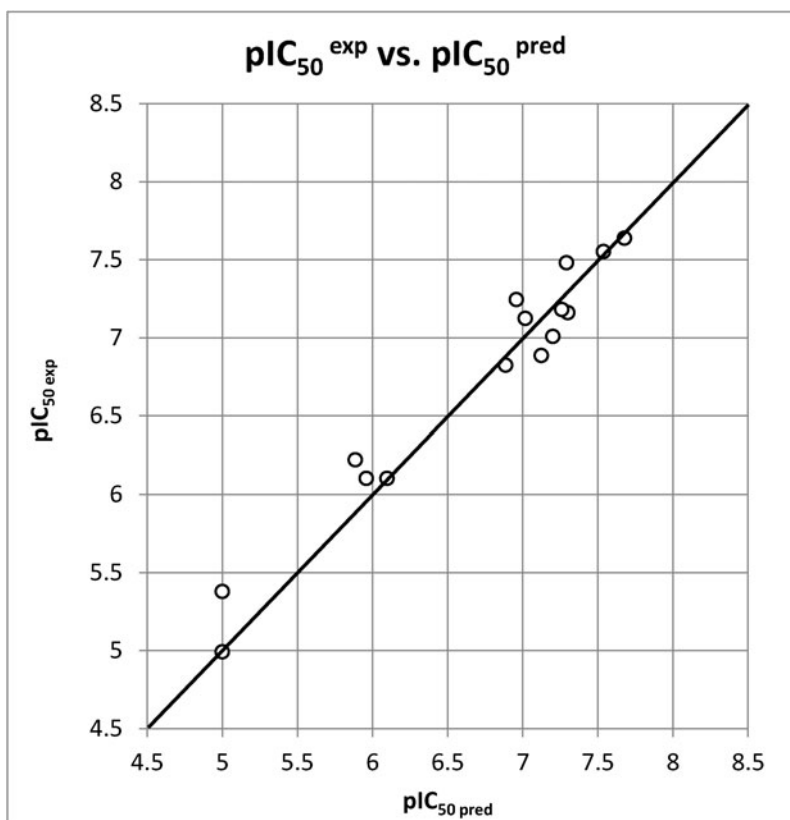
Figure 7. The correlation plot of experimental vs. predicted inhibitory activity for the Hypo1 pharmacophore.

and the chemical structures of the analogues are shown on Figure 9 and listed in Table 4. The first nine rows of Table 4 refer to the best virtually proposed TCL analogues with highest predicted inhibitory activities against the *Pf*ENR.[23] The estimated inhibitory potencies of the analogues against both enzymes suggest that the inhibitory activities are of about the same order for 5 of them, indicating that design of triclosan derivatives against dual targets by QSAR analysis is feasible.

The absence of aromatic fragments in R_1-group of the reference ligand Triclosan (TCL1, Table 1, with IC_{50}^{exp} of 1100 nM (InhA of *Mtb*) and 73 nM (*Pf*ENR)[19,30–32]) could explain its mild *in vitro* activity against the InhA.[19] Indeed the most active TCL analogue, namely TCL11 with R_1-group equal to $(CH_2)_2$Ph (Table 1, IC_{50}^{exp} of 21 nM for InhA of *Mtb* and 76 nM for *Pf*ENR[19,30–32]) is three times more potent against the *Mtb* InhA than the *Pf*ENR. This significant increase of potency from TCL1 to TCL11 indicates the sensitivity of *Mtb* InhA to the presence of bulkier hydrophobic R_1-group while the inhibitory potency against the *Pf*ENR remains basically unchanged, provided that the R_1-group contains an aromatic ring linked to the TCL scaffold via short aliphatic linker (TCL10, TCL11, Table 1).

In our former study on *Pf*ENR inhibition[23] the strongest interactions of TCLs with the enzyme were predicted for

analogues with the following *R*-groups: $R_1\equiv38$ and 40; $R_2\equiv9$ and 13; $R_3\equiv11$ and 9 (Figure 8). The current complexation model relying on $\Delta\Delta G_{com}$ computed for TCLs interacting with InhA of *Mtb* predicted the highest affinity for TCLs with $R_1\equiv25, 36, 38$ and 40; $R_2\equiv10, 13, 18, 23$ and $R_3\equiv4, 9, 10, 11$ (Table 4, Figures 8 and 9). The analogue TCL-40-13-9 (Figure 9) is one of the most interesting dual inhibitors with similar predicted inhibitory potencies against the InhA of *Mtb* and *Pf*ENR in low nanomolar concentration range (20 and 14 nM, respectively, Table 4). Likewise, TCL-38-10-4 displays predicted potencies of 10 and 30 nM (Table 4). Its dihydrobenzofuran group ($R_1\equiv38$) fills the same hydrophobic pocket (Figure 5D) like $R_1\equiv40$, as shown for TCL-40-9-11 on Figure 5B. The aromatics rings of R_1-groups 36 till 40 form stacking $\pi-\pi$ interactions with the phenyl ring of the catalytic Tyr158 as displayed on Figure 5C for the analog TCL-36-23-9. The cyclohexyl ring ($R_1\equiv33$) does not have the capacity to form $\pi-\pi$ interactions but it fills well the hydrophobic pocket of InhA, as documented by the low predicted IC_{50}^{pre} of 24 nM, Table 4, for the analog TCL-33-23-10. The *m*-xylene group of $R_1\equiv25$ with too short aliphatic linker obviously cannot reach into this hydrophobic pocket. The InhA of *Mtb* seems to prefer an aromatic substituent in the R_2-group such as the phenyl group of $R_2\equiv23$, which can form a favorable stacking interaction with the near Phe97,

Table 4. Virtually Proposed analogs with predicted inhibitory activities against *Pf*ENR[23] and InhA of *Mtb* (in nM).

Analog [a]	M_w [b]	$\triangle\triangle H_{MM}$ [c]	$\triangle\triangle G_{sol}$ [d]	$\triangle\triangle TS_{vib}$ [e]	$\triangle\triangle G_{com}$ [f]	IC_{50}^{pre} [g] InhA	IC_{50}^{pre} [h] *Pf*ENR
TCL-33-17-10	368	−37.77	19.49	4.58	−13.70	112	37
TCL-37-7-3	364	−23.53	4.06	−0.37	−19.84	44	50
TCL-37-9-11	377	−27.40	13.68	1.34	−12.38	137	42
TCL-38-4-7a	387	−21.45	2.64	−0.07	−18.88	51	55
TCL-38-10-4b	391	−23.30	−8.18	1.73	−29.76	10	30
TCL-39-6-11	394	−21.63	5.41	0.22	−16.00	79	37
TCL-40-9-11	425	−31.06	10.79	2.05	−18.22	57	13
TCL-40-13-9	428	−32.17	7.73	−0.79	−25.23	20	14
TCL-40-14-10	412	−54.52	40.48	1.57	−12.48	135	40
TCL-25-18-9	346	−36.88	13.58	4.50	−18.80	52	74
TCL-25-18–10	347	−39.34	13.51	5.14	−20.7	39	75
TCL-25-18-11	361	−51.77	20.18	8.72	−22.86	28	32
TCL-25-22-9	375	−45.32	28.26	4.94	−12.11	143	41
TCL-25-22-10	376	−43.03	13.21	6.44	−23.37	26	42
TCL-25-22-11	390	−35.47	15.18	9.25	−11.04	168	17
TCL-25-23-9	380	−40.28	9.29	2.85	−28.14	13	22
TCL-25-23-10	381	−39.04	12.83	2.31	−23.89	24	79
TCL-25-23-11	395	−32.97	5.01	0.45	−27.51	14	36
TCL-33–18–9	353	−12.31	8.62	5.10	1.42	1104	68
TCL-33-18-10	354	−13.35	−3.43	5.53	−11.25	162	92
TCL-33-18-11	368	−30.81	13.94	8.70	−8.17	259	47
TCL-33-22-9	381	−31.55	21.81	9.80	0.06	899	65
TCL-33-22-10	382	−14.85	12.30	9.74	7.19	2644	60
TCL-33-22-11	396	−15.25	9.60	11.06	5.41	2019	41
TCL-33-23-9	387	−22.35	−0.57	2.54	−20.38	41	41
TCL-33-23-10	388	−21.68	−4.81	2.54	−23.95	24	22
TCL-33-23-11	402	−21.12	2.70	5.89	−12.53	134	28
TCL-36-18-9	361	−27.68	6.21	1.41	−20.06	43	121
TCL-36-18-10	362	−25.89	−1.82	0.90	−26.81	15	144
TCL-36-18-11	376	−28.10	5.52	2.66	−19.91	44	79
TCL-36-22-9	390	−30.19	6.13	2.06	−22.01	32	103
TCL-36-22-10	391	−29.23	6.72	1.36	−21.14	36	114
TCL-36-22-11	405	−30.15	12.13	2.97	−15.05	91	47
TCL-36-23-9	395	−36.24	7.26	−3.29	−32.27	7	52
TCL-36-23-10	396	−35.11	8.05	−2.39	−29.45	10	60
TCL-36-23-11	411	−23.02	8.61	−1.90	−16.31	76	18

[a] The numbering of new analogues TCL-X-Y-Z is formulated as in Ref. [23]: X correspond to the R_1-group number, Y to R_2-group number and finally Z to R_3-group number, [b]–[f] see Tables 1 and 2, [g] IC_{50}^{pre} was calculated from Correlation Equation 7, Table 3, [h] Taken from V. Frecer et al.[23] and V. Frecer, E. Megnassan, S. Miertus, unpublished results.

Table 5. Output parameters of 10 generated PH4 pharmacophoric hypotheses for InhA inhibitors after CatScramble validation procedure.

Hypothesis	RMSD [a]	R^2 [b]	Total costs [c]
Hypo1	2.067	0.88	62.1
Hypo2	3.155	0.71	99.3
Hypo3	3.202	0.71	101.1
Hypo4	3.530	0.64	116.1
Hypo5	3.672	0.61	124.7
Hypo6	3.852	0.56	131.6
Hypo7	3.996	0.53	141.0
Hypo8	4.004	0.53	142.4
Hypo9	4.036	0.52	143.3
Hypo10	4.148	0.49	148.0
Fixed Cost	0	1.0	34.2
Null Cost	5.833	0	244.2

[a] root mean square deviation; [b] correlation coefficient; [c] overall cost parameter of the PH4 pharmacophore.

as depicted in Figure 5C for the analog TCL-36-23-9 with IC_{50}^{pred} of 7 nM. In the training set of TCL analogs the R_3-group was not derivatized, which restricted the variability of these substituents only to the chlorine atoms isosteres. Among them ethyl ($R_3 \equiv 9$), methylamine ($R_3 \equiv 10$) and dimethylamine ($R_3 \equiv 11$) appeared to form the best substituents (Table 4).

While the best virtually proposed TCL analogs with the highest predicted inhibitory potencies against the InhA of *Mtb* are TCL-36-23-9 ($IC_{50}^{pre} = 7$ nM), TCL-38-10-4 ($IC_{50}^{pre} = 10$ nM) and TCL-36-23-10 ($IC_{50}^{pre} = 10$ nM), the best identified dual target inhibitors include TCL-40-13-9, TCL-38-10-4 and TCL-25-23-9, Table 4.
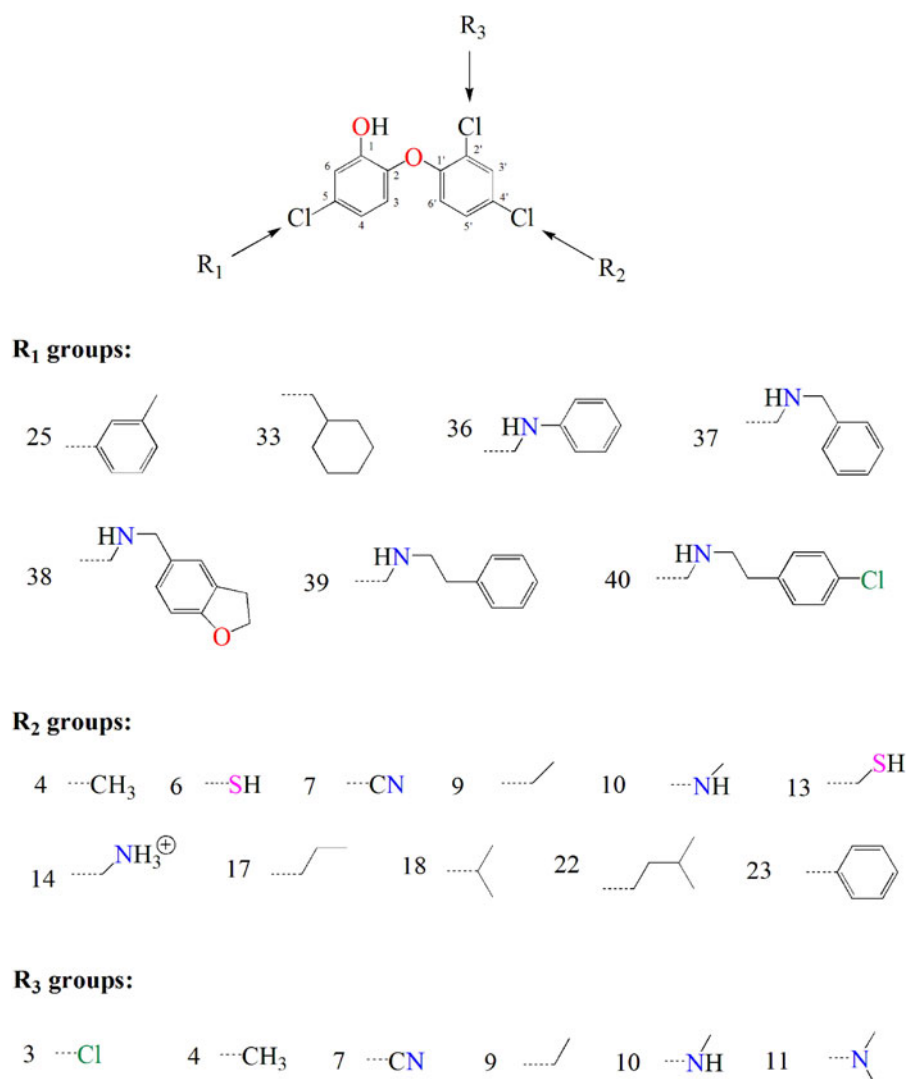
Figure 8. The molecular scaffold and R-groups (R_1, R_2 and R_3) of virtual library of TCL analogs, which were explored as potential inhibitors of the InhA of *Mtb*.

3 Conclusions

The complexation QSAR model for reversible inhibitors employing Gibbs free energy of enzyme-inhibitor interactions computed for complexes of TCL$_x$: InhA of *Mtb* was validated by the PH4 pharmacophore model derived from a training set of TCLs with observed inhibitory potencies. Structural information and estimated inhibitory activities of previously designed virtual library of TCLs[23] predicted to inhibit the *Pf*ENR directed us in our effort to identify predicted nanomolar dual target inhibitors predicted to bind *Pf*ENR as well as InhA of *Mtb* by enhanced active site interactions as compared to the TCLs of the training set. Especially the TCL-36-23-9 with predicted low nanomolar IC_{50}^{pre} of 7 nM against InhA of *Mtb* and potential dual target inhibitor TCL-25-23-9 with predicted potencies $IC_{50}^{pre} = 13$ nM (InhA of *Mtb*) and $IC_{50}^{pre} = 22$ nM (*Pf*ENR) can be proposed for synthesis and subsequent activity evaluation in enzy-

matic assays, which may lead to discovery of novel antituberculotic and antimalarial compounds.

4 Experimental

4.1 Training and Validation Sets

The training and validation sets of triclosan analogue inhibitors of InhA of *Mtb* used in this study were selected from literature.[19,30–32] The inhibitory potencies of these derivatives cover a sufficiently broad range of activities to allow a reliable QSAR model to be built ($21 \leq IC_{50} \leq 1100$ nM).

4.2 Model Building

Molecular models of the enzyme-inhibitor complexes (E:I), free InhA (E) and inhibitors (I) were prepared from the
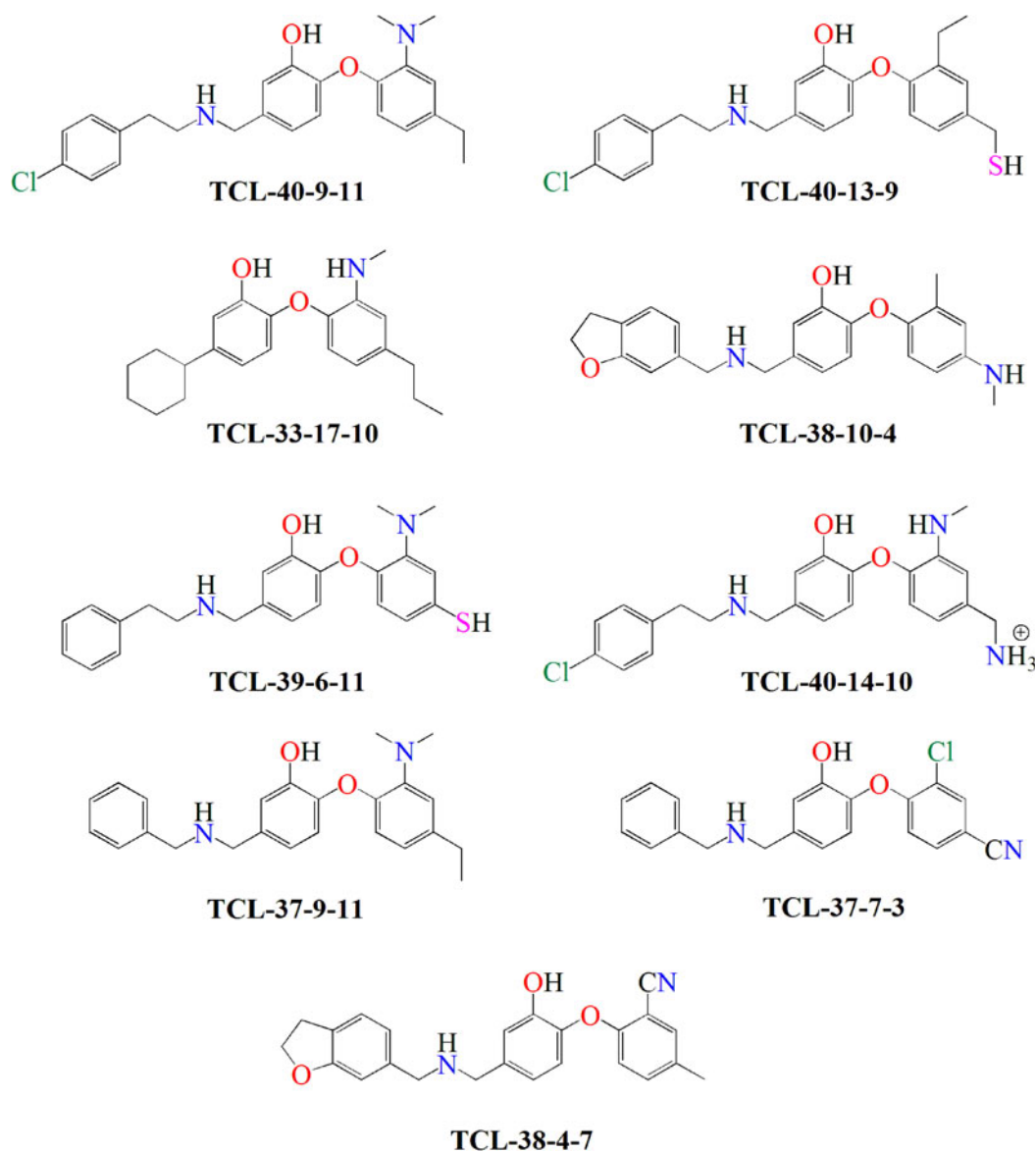
Figure 9. Chemical structures of selected analogs from highly focused combinatorial subset of a virtual library of TCL analogs (Table 4) evaluated for inhibitory potencies against *Pf*ENR[23] and tested for inhibition of InhA of *Mtb* by the complexation QSAR model.

high-resolution crystal structure of the reference complex InhA:TCL containing the triclosan bound to InhA[12] (Protein Data Bank[30] entry code 1P45 at a resolution of 2.6 Å) using Insight-II molecular modeling program.[31]

The structures of the *E* and *E:I* complexes were considered at appropriate physiologically relevant pH of 7 with capped neutral N- and C-terminal residues and all protonated and ionized residues charged. No crystallographic water molecules were included into the model. The inhibitors were built into the reference structure complex by in situ replacement of the derivatized *R*-groups of the TCL moiety (scaffold). An exhaustive conformational search over all rotatable bonds of the replacing function group coupled with a careful gradual energy-minimization of the modified inhibitor and the InhA active site residues located in the vi-

cinity of the inhibitor (within 5 Å distance), was employed to identify the low-energy bound conformations of the modified inhibitor. The resulting low-energy structures of the *E:I* complexes were then carefully refined by minimization of the whole complex. This procedure has been previously successfully used for model building of viral, bacterial and protozoal protease-inhibitor complexes and design of peptidomimetic, hydroxynaphthoic and thymidine-based inhibitors.[24–26,28,29,32,33]

4.3 Molecular Mechanics

Simulations of the models of inhibitors, InhA and their complexes were carried out with an all-atom representation using atomic and charge parameters of the class II consis-
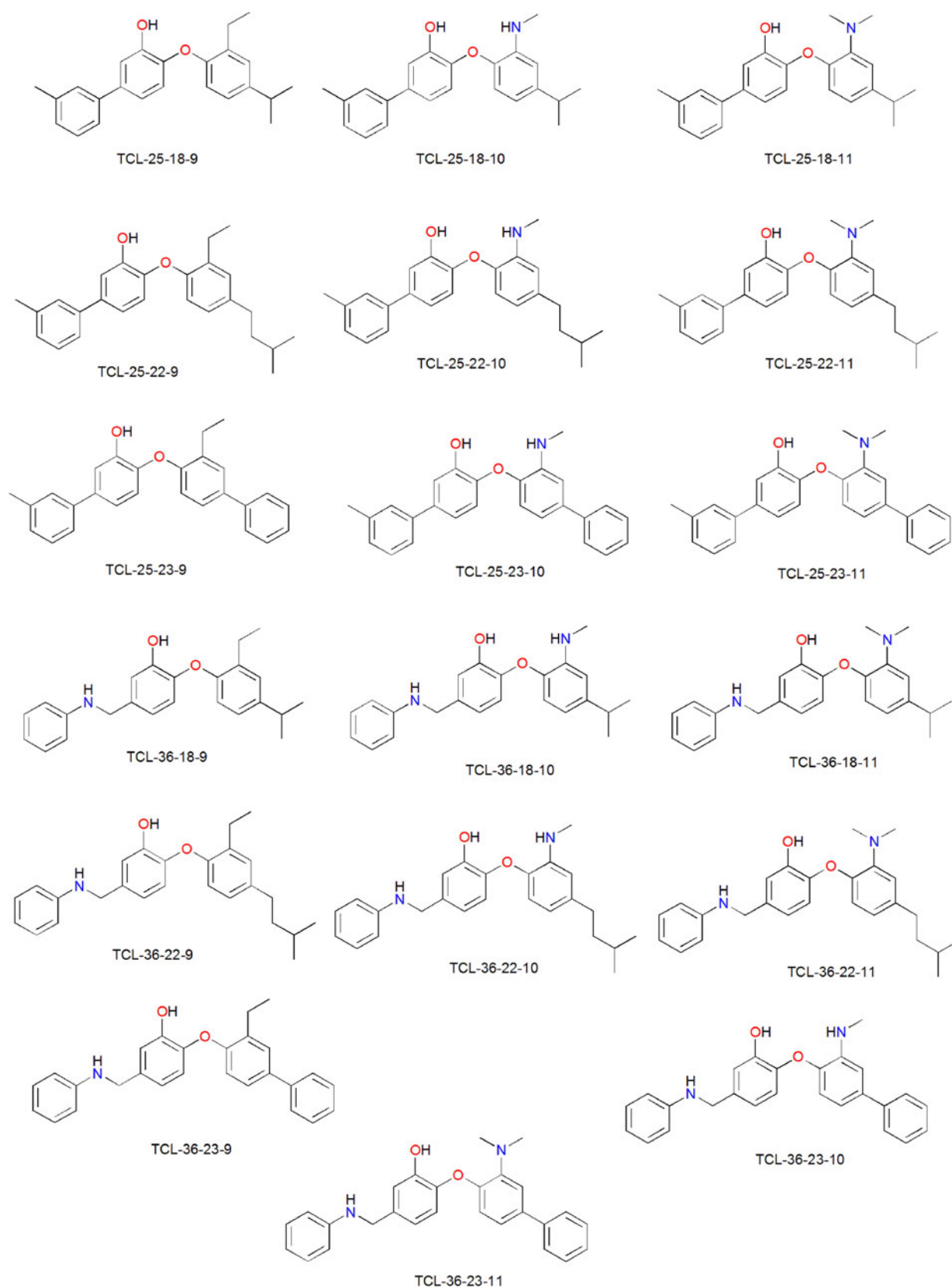
TCL-25-18-9

TCL-25-18-10

TCL-25-18-11

TCL-25-22-9

TCL-25-22-10

TCL-25-22-11

TCL-25-23-9

TCL-25-23-10

TCL-25-23-11

TCL-36-18-9

TCL-36-18-10

TCL-36-18-11

TCL-36-22-9

TCL-36-22-10

TCL-36-22-11

TCL-36-23-9
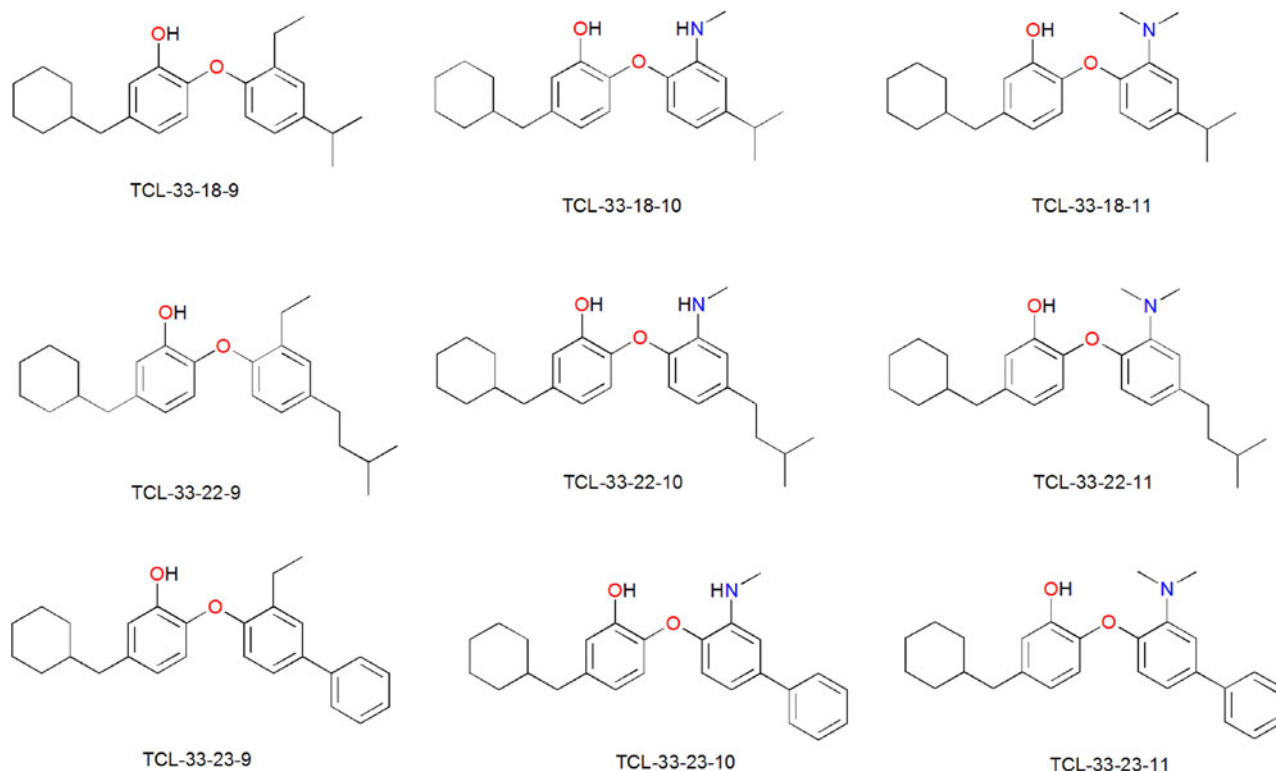
TCL-36-23-10

TCL-36-23-11

Figure 9 (Continued)

Figure 9 (Continued)

tent force field CFF91.[34] A dielectric constant of 4 was used for all molecular mechanics (MM) calculations in order to take into account the dielectric shielding effect in proteins. Minimizations of the *E:I* complexes, free *E* and *I* were carried out by relaxing the structures gradually, starting with added hydrogen atoms, continued with residue side chain heavy atoms and followed by the protein backbone relaxation. In all the geometry optimizations, a sufficient number of steepest descent and conjugate gradient iterative cycles were used with the convergence criterion for the average gradient set to 0.01 kcal mol^{-1} Å^{-1}.

4.4 Conformational Search

Free inhibitor conformations were derived from their bound conformations in the *E:I* complexes by gradual relaxation to the nearest local energy minimum. This was followed by a Monte Carlo search (with an upper limit of 50 000 iterations) for low-energy conformations over all rotatable bonds except for those in the rings which were carried out using a Cerius^2 molecular modeling package.[35] Two hundred unique conformations were generated for each inhibitor by randomly varying torsion angles of the last accepted conformer by ±15° at 5000 K, followed by subsequent energy minimization. During the minimization a dielectric constant $\varepsilon = 80$ was used to account approximately for the dielectric screening effect of hydration upon

the generated conformers. The conformer with the lowest total energy was selected and re-minimized at $\varepsilon = 4$.

4.5 Solvation Gibbs Free Energies

The electrostatic component of solvation Gibbs free energy that also incorporates the effects of ionic strength via solving the solution of the nonlinear Poisson–Boltzmann equation[36,37] was computed by the DelPhi module in the Discovery Studio.[38] The program treats the solvent as a continuous medium of high dielectric constant ($\varepsilon_o = 80$) and the solute as a cavity of low dielectric ($\varepsilon_i = 4$) with boundaries linked to the solute's molecular surface, which encloses the solute's atomic charges. The program uses a finite difference method to numerically solve for the molecular electrostatic potential and reaction field around the solute. DelPhi calculations were carried out on a ($235 \times 235 \times 235$) cubic lattice grid for the *E:I* complexes and free enzyme and a ($65 \times 65 \times 65$) grid for the free *I* with full coulombic boundary conditions. Two subsequent focusing steps led in both cases to a similar final resolution of about 0.3 Å per grid unit at 70 % filling of the grid by the solute. Physiological ionic strength of 0.145 mol dm^{-3}, atomic partial charges and radii defined in the CFF parameter set[37] and a probe sphere radius of 1.4 Å were used. The electrostatic component of the solvation Gibbs free energy was calculated as the reaction field energy.[39–41]

4.6 Entropic Term

The vibrational entropy change during the inhibitor binding to the enzyme was calculated by normal mode analysis of the inhibitor vibrations using the simplified method of Fischer et al.[42,43] In this approach, vibrational analysis of the inhibitor bound at the active site of a 'frozen' receptor (*E*) and of the low-energy conformer of the free inhibitor are computed for fully minimized structures using Discover[34] and $\Delta TS_{vib} = \Delta TS_{vib}\{I_x\}_E - \Delta TS_{vib}\{I_x\}$ It has been shown previously that for small and relatively stiff ligands this method gives a good approximation of the vibrational entropy change of the fully flexible system, i.e. including the degrees of freedom of the protein receptor.[45,46] The $\Delta TS_{vib}\{I_x\}$ term accounts for vibrational motions of the free inhibitor and represents an indicator of conformational flexibility of the molecule. Low frequency vibrations, which correspond to collective motions of a number of atoms with larger amplitudes, i.e. conformational changes, contribute most to this term. Relative values of $\Delta\Delta TS_{vib}$ with respect to a reference inhibitor were used to compensate partially for the restricted flexibility of the enzyme. Although an enthalpic contribution to binding affinity is essential, the entropy term is recognized as an important factor for drug optimization.[44]

4.7 Calculation of Binding Affinity

Half maximal inhibitory concentration (IC_{50}) of a reversible inhibitor *I* is related to the standard Gibbs free energy (GFE) change of the formation of the *E:I* complex (ΔG_{com}) in a solvent. The IC_{50} value can thus be predicted from the complexation GFE as $\Delta G_{com} = -RT \ln(IC_{50})$, assuming the following equilibrium:

$$\{E\}_{aq} + \{I\}_{aq} \leftrightarrow \{E:I\}_{aq} \tag{1}$$
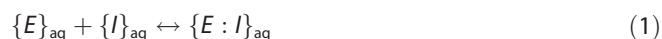
Where $\{X\}_{aq}$ indicates solvated species *X*. The standard GFE change of Reaction 1 can be derived by molecular simulations of the complex and the free reactants[24]

$$\Delta G_{com} = G(E:I) - G\{E\} - G\{I\} \tag{2}$$

In this work we approximate the exact values of standard GFE for larger systems such as enzyme:inhibitor complexes by the expression[24–26]:

$$G(E:I) \approx E_{MM}\{E:I\} + RT - TS_{trv}\{E:I\} + G_{sol}\{E:I\} \tag{3}$$

where $E_{MM}\{E:I\}$ stands for the molecular mechanics total energy of the complex (including bonding and non-bonding contributions), $G_{sol}\{E:I\}$ is the solvation GFE and $TS_{trv}\{E:I\}$ is the entropic term:

$$TS_{trv}\{E:I\} = TS_{tran}\{E:I\} + TS_{rot}\{E:I\} + TS_{vib}\{E:I\} \tag{4}$$

composed of a sum of contributions arising from translational, rotational and vibrational motions of *E:I*, respectively. Assuming that the translational and rotational terms for the free *E* and the complex *E:I* are approximately equal, we obtain:

$$\Delta G_{com} \approx [E_{MM}\{E:I\} - E_{MM}\{E\} - E_{MM}\{I\}] + [G_{sol}\{E:I\} - G_{sol}\{E\}$$
$$- G_{sol}\{I\}] + TS_{tran}\{I\} + TS_{rot}\{I\} - [TS_{vib}\{E:I\}$$
$$- TS_{vib}\{E\} - TS_{vib}\{I\}] = \Delta H_{MM} + TS_{tran}\{I\}$$
$$+ TS_{rot}\{I\} - \Delta TS_{vib} + \Delta G_{sol} \tag{5}$$

where $TS_{tran}\{I\}$ and $TS_{rot}\{I\}$ describe the translational and rotational entropy terms of the free inhibitor and ΔTS_{vib} represents the vibrational entropy change upon the complex formation.

Comparison between different inhibitors was done via relative changes in the complexation GFE with respect to a reference inhibitor, I_{ref}, assuming ideal gas behavior for the rotational and translational motions of the inhibitors:

$$\Delta\Delta G_{com} = \Delta G_{com}\{I\} - \Delta G_{com}\{I_{ref}\} = \Delta\Delta H_{MM} - \Delta\Delta TS_{vib} + \Delta\Delta G_{sol} \tag{6}$$

The evaluation of relative changes is preferable as it is expected to lead to partial cancellation of errors caused by the approximate nature of the molecular mechanics method and the solvent and entropic effects description.

4.8 Pharmacophore Generation

Pharmacophore modeling assumes that a set of structural features in a molecule is recognized at the receptor site and is responsible for the molecule's biological activity. Bound conformations of inhibitors taken from the models of *E:I* complexes were used for the building of the 3D-QSAR pharmacophore by means of the Catalyst HypoGen algorithm[45] implemented in Discovery Studio.[41] The top scoring pharmacophore hypothesis was built up in three stages (constructive, subtractive and optimization step) from the set of most active inhibitors. Inactive molecules served for definition of the excluded volume. The maximum number of five features allowed by the HypoGen algorithm was selected based on the TCL scaffold and substituents during the pharmacophore generation, namely: hydrophobic aromatic (HYdAr), hydrophobic aliphatic (HYd), hydrogen-bond donor, (HBD), hydrogen-bond acceptor (HBA) and ring aromatic (Ar). Adjustable parameters of the protocol were kept at their default values except the uncertainty on the activity, which was set to 1.25 instead of 3. This last choice to bring the uncertainty interval on experimental activity from the large $<IC_{50}/3, 3 \times IC_{50}>$ to a relatively narrow $<4 \times IC_{50}/5, 5 \times IC_{50}/4>$ taking thus into account the accuracy and homogeneity of the measured inhibitory activities measured by the same method in a single laboratory. During the generation of 10 pharmaco-

phores the number of missing features was set to 0 and the best pharmacophore was selected. The generated pharmacophore models were assessed for their reliability based on the calculated cost parameters. The overall costs of a model consist of three components: (i) the weight cost, (ii) the error cost, and (iii) the configuration cost. Three additional costs: (i) the fixed cost, (ii) the total cost, and (iii) the null cost are calculated during the pharmacophore generation. The fixed cost represents the lowest possible cost of the simplest pharmacophore model that ideally fits the data. Fixed costs are calculated by summing up the minimum possible error and weight cost plus the constant configuration cost. A further cost parameter; the null cost, stands for the maximum cost of a pharmacophore with no features and corresponds to the averaged activity data of the training set molecules.

Acknowledgements

References

[1] *Global Tuberculosis Control*, WHO Report 2010, pp. 1–42, WHO Press, Geneva, Switzerland, **2010**; ISBN 978-92-4-156406-9.

[2] World Health Organization, *TDR News No. 85*, May **2010**, WHO, Geneva, Switzerland, **2010**.

[3] http://onlinelibrary.wiley.com/doi/10.1002/14651858. CD003343.pub3/abstract.

[4] D. J. Girling, *Tubercle* **1978**, *59*, 13–32.

[5] M. Asif, *Int. J. Pharmaceut. Chem.* **2012**, *2*, 110–120.

[6] a) K. Sharma, P. Chopra, Y. Singh, *Expert Opin. Ther. Targets* **2004**, *8*, 79–93; b) N. Minovski, A. Perdih, M. Novic, T. Solmajer, *J. Comput. Chem.* **2013**, *34*(9), 790–801; c) N. Minovski, A. Perdih, T. Solmajer, *J. Mol. Model.* **2012**, *18*(5), 1735–1753

[7] J. W. Campbell, J. E. Cronan Jr, *Annu. Rev. Microb.* **2001**, *55*, 305–332.

[8] R. J. Heath, C. O. Rock, *Curr. Opin. Invest. Drugs* **2004**, *5*, 46–153.

[9] S. W. White, J. Zheng, Y. M. Zhang, C. O. Rock, *Annu. Rev. Biochem.* **2005**, *74*, 791–831.

[10] Y. M. Zhang, Y. J. Lu, C. O. Rock, *Lipids* **2004**, *39*, 1055–1060.

[11] H. T. Wright, K. A. Reynolds, *Curr. Opin. Microbiol.* **2007**, *10*, 447–453.

[12] M. R. Kuo, H. R. Morbidoni, D. Alland, S. F. Sneddon, B. B. Gourlie, M. M. Staveski, M. Leonard, J. S. Gregory, A. D. Janjigian, C. Yee, J. M. Musser, B. Kreiswirth, H. Iwamoto, R. Perozzo, W. R. Jacobs Jr., J. C. Sacchettini, D. A. Fidock, *J. Biol. Chem.* **2003**, *278*, 20851–20859.

[13] S. Parikh, D. P. Moynihan, G. Xiao, P. J. Tonge, *Biochemistry* **1999**, *38*, 13623–13634.

[14] E. K. Schroeder, L. A. Basso, D. S. Santos, O. N. de Souza, *Biophys. J.* **2005**, *89*, 1–9.

[15] E. K. Schroeder, O. N. de Souza, D. S. Santos, J. S. Blanchard, L. A. Basso, *Curr. Pharm. Biotechnol.* **2002**, *3*, 197–225.

[16] A. E. DeBarber, K. Mduli, M. Bosman, L. G. Bekker, C. E. Barry 3rd, *Proc. Natl. Acad. Sci. USA* **2000**, *97*, 9677–9682.

[17] G. P. Morlock, B. Metchock, D. Sikes, J. T. Crawford, R. C. Cooksey, *Antimicrob. Agents Chemother.* **2003**, *47*, 3799–3805.

[18] R. Rawat, A. Whitty, P. J. Tonge, *Proc. Natl. Acad. Sci. USA* **2003**, *100*, 13881–13886.

[19] J. S. Freundlich, F. Wang, C. Vilchèze, G. Gulten, R. Langley, G. A. Scheihser, D. P. Jacobus, W. R. Jacobs Jr., J. C. Sacchettini, *ChemMedChem* **2009**, *4*, 241–248.

[20] J. S. Freundlich, F. Wang, H.-C. Tsai, M. Kuo, H.-M. Shieh, J. W. Anderson, L. J. Nkrumah, J.-C. Valderramos, M. Yu, T. R. S. Kumar, S. G. Valderramos, W. R. Jacobs Jr., G. A. Schiehser, D. P. Jacobus, D. A. Fidock, J. C. Sacchettini, *J. Biol. Chem.* **2007**, *282*, 25436–25444.

[21] R. Perozzo, M. Kuo, A. S. Sidhu, J. T. Valiyaveettil, R. Bittman, W. R. Jacobs Jr., D. A. Fidock, J. C. Sacchettini, *J. Biol. Chem.* **2002**, *277*, 13106–13114.

[22] M. Kapoor, C. C. Reddy, M. V. Krishnasastry, N. Surolia, A. Surolia, *Biochem. J.* **2004**, *381*, 719–724.

[23] V. Frecer, E. Megnassan, S. Miertus, *Eur. J. Med. Chem.* **2009**, *44*, 3009–3019.

[24] V. Frecer, S. Miertus, A. Tossi, D. Romeo, *Drug Des. Disc.* **1998**, *15*, 211–231.

[25] V. Frecer, F. Berti, F. Benedetti, S. Miertus, *J. Mol. Graph. Model.* **2008**, *27*, 376–387.

[26] V. Frecer, M. Kabelac, P. De Nardi, S. Pricl, S. Miertus, *J. Mol. Graph. Model.* **2004**, *22*, 209–220.

[27] V. Frecer, P. Seneci, S. Miertus, *J. Comput. Aided Mol. Des.* **2011**, *25*, 31–49.

[28] L. C. Owono Owono, M. Keita, E. Megnassan, V. Frecer, S. Miertus, *Tuberc. Res. Treat.* **2013**, 670836

[29] B. Dali, M. Keita, E. Megnassan, V. Frecer, S. Miertus, *Chem. Biol. Drug. Des.* **2012**, *79*(4), 411–430.

[30] J. S. Freundlich, J. W. Anderson, D. Sarantakis, H. M. Shieh, M. Yu, J. C. Valderramos, E. Lucumi, M. Kuo, W. R. Jacobs Jr., D. A. Fidock, G. A. Schiehser, D. P. Jacobus, J. C. Sacchettini, *Bioorg. Med. Chem. Lett.* **2005**, *15*(23), 5247–5252.

[31] J. S. Freundlich, M. Yu, E. Lucumi, M. Kuo, H. C. Tsai, J. C. Valderramosb, L. Karagyozov, W. R. Jacobs Jr., G. A. Schiehser, D. A. Fidock, D. P. Jacobus, J. C. Sacchettini, *Bioorg. Med. Chem. Lett.* **2006**, *16*(8), 2163–2169.

[32] J. S. Freundlich, F. Wang, H. C. Tsai, M. Kuo, H. M. Shieh, J. W. Anderson, L. J. Nkrumah, J. C. Valderramos, M. Yu, T. R. Santha Kumar, S. G. Valderramos, W. R. Jacobs Jr., G. A. Schiehser, D. P. Jacobus, D. A. Fidock, J. C. Sacchettini, *J. Biol. Chem.* **2007**, *282*(35), 25436–25444.

[33] H. M. Berman, J. Westbrook, Z. Feng, G. Gilliland, T. N. Bhat, H. Weissig, I. N. Shindyalov, P. E. Bourne, *Nucleic Acids Res.* **2000**, *28*, 235–42.

[34] *Insight-II and Discover molecular modeling and simulation package*, Version 2005, Accelrys, Inc., San Diego, CA, **2005**.

[35] E. Megnassan, M. Keita, C. Bieri, A. Esmel, V. Frecer, S. Miertus, *Med. Chem.* **2012**, *8*, 970–984.

[36] M. Keita, A. Kumar, B. Dali, E. Megnassan, M. I. Siddiqi, V. Frecer, S. Miertus, *RSC Adv.* **2014**, *4*, 55853–55866

[37] J. R. Maple, M. J. Hwang, T. P. Stockfish, U. Dinur, M. Waldman, C. S. Ewig, A. T. Hagler, *J. Comput. Chem.* **1994**, *15*, 162–182.

[38] *Cerius² Life Sciences molecular simulation software*, Version 4.6, Accelrys Inc., San Diego, CA, **2002**.

[39] M. K. Gilson, B. Honig, *J. Comput. Aided Mol. Des.* **1991**, *5*, 5–20.

[40] W. Rocchia, S. Sridharan, A. Nicholls, E. Alexov, A. Chiabrera, B. Honig, *J. Comput. Chem.* **2002**, *23*, 128–37.

[41] D*iscovery Studio molecular modeling and simulation program*, Version 2.5, Accelrys, Inc., San Diego, CA, **2009**.

[42] C. J. F. Böttcher in *Theory of Electric Polarization*, Elsevier, Amsterdam, **1973**.

[43] S. Miertus, E. Scrocco, J. Tomasi, *Chem. Phys.* **1981**, *55*, 117–129.

[44] V. Frecer, S. Miertus, *Int. J. Quantum Chem.* **1992**, *42*, 1449–1468.

[45] S. Fischer, J. C. Smith, C. S. Verma, *J. Phys. Chem. B* **2001**, *105*, 8050–8055.

[46] S. M. Schwarzl, T. B. Tschopp, J. C. Smith, S. Fischer, *J. Comput. Chem.* **2002**, *23*, 1143–1149.

[47] E. Freire, *Drug. Discov. Today* **2008**, *13*, 869–874.

[48] H. Li, J. Sutter, R. Hoffmann, in *Pharmacophore Perception, Development and Use in Drug Design* (Ed: O. F. Güner), International University Line, La Jolla, CA, **2000**, pp. 171–189.